Mixed Oligoureas Based on Constrained Bicyclic and Acyclic β-Amino Acids Derivatives: On the Significance of the Subunit Configuration for Folding

Christophe André,[a] Baptiste Legrand,[a] Laure Moulat,[a] Emmanuel Wenger,[b] Claude Didierjean,[b] Emmanuel Aubert,[b] Marie Christine Averlant-Petit,[c] Jean Martinez,[a] Muriel Amblard,*[a] and Monique Calmes*[a]

Abstract: The combination of a non-functionalized constrained bicyclo-[2.2.2]octane motif along with urea linkages allowed the formation of a highly rigid $2.5_{12/14}$ helical system both in solution and the solid state. In this work, we aimed at developing stable and functionalized systems as promising materials for biological applications in investigating the impact of this constrained motif and its configuration on homo and heterochiral mixed-oligourea helix formation. Di-, tetra-, hexa-, and octa-oligoureas alternating the highly constrained bicyclic motif of (R) or (S) configuration with acyclic (S)-β³-amino acid derivatives were constructed. Circular dichroism (CD), NMR experiments, and the X-ray crystal structure of the octamer unequivocally proved that the alternating heterochiral R/S sequences form a stable left-handed 2.5-helix in contrast to the mixed (S/S)-oligoureas, which did not adopt any defined secondary structure. We observed that the (−)-synclinal conformation around the C_α−C_β bond of the acyclic residues, although sterically less favorable than the (+)-synclinal conformation, was imposed by the (R)-bicyclic amino carbamoyl (BAC) residue. This highlighted the strong ability of the BAC residue to drive helical folding in heterochiral compounds. The role of the stereochemistry of the BAC unit was assessed and a model was proposed to explain the misfolding of the S/S sequences.

Keywords: bicyclic β-amino acid derivatives · conformation analysis · foldamers · mixed oligoureas · helical structures

Introduction

The ability of β- and γ-amino acid oligomers to adopt protein-like secondary structures has emerged as a particularly attractive field of research to design well-defined secondary structures that can mimic natural structural motifs of biomolecules.[1,2] The use of amino acid homologues, commonly derived from natural α-amino acids, allowed the design of various helical systems (i.e., 14-, 12-, 10/12-helix), which are substantially enlarged with homo- and heterochiral constrained cyclic derivatives as well as the combination of α-, β-, and γ- amino acids to synthesize α/β, α/γ, β/γ sequences of a particular folding.[3] Although a broad range of amide-based structures has been described with various combinations, the link between building blocks was not so intensively explored. Among the different possibilities of amino acid derivative connections, the urea linkage presents a particularly interesting bifurcated hydrogen-bond stabilization system. This linkage has received a particular attention by the group of Guichard,[4–8] and was mainly applied to acyclic β-amino acid derivative foldamers. Recently, we explored the propensity of oligourea incorporating a highly constrained bicyclic β-amino acid ((S)-aminobicyclo[2.2.2]octane-2-carboxylic acid; (S)-ABOC) to adopt stable discrete secondary structures.[9,10] The resulting bicyclic amino carbamoyl homo-oligoureas (BAC oligoureas) displayed a highly rigid $2.5_{12/14}$ helical structure both in solution and in the solid state.[10] Importantly, even in solution, no critical sequence size was needed to initiate the folding in BAC oligoureas, and no isomerization of the urea bond was detected. This first series of BAC homo-oligoureas provides the basis for designing stable functionalized foldamers for biological applications, in particular for the inhibition of protein–protein interactions.[11] However, to develop BAC-based oligoureas containing specific side-chains, mixed systems must be used. In such systems the BAC residue will be used for its high folding propensity in combination with building blocks containing proteogenic (or non proteogenic) amino acid side-chains. For that purpose, we focused our attention on the

[a] Dr. C. André,⁺ Dr. B. Legrand,⁺ L. Moulat, Prof. J. Martinez, Dr. M. Amblard, Dr. M. Calmes
IBMM, UMR 5247 CNRS, Universités Montpellier 1 et 2
15 avenue Charles Flahault, 34093 Montpellier Cedex 5 (France)
E-mail: muriel.amblard@univ-montp1.fr
monique.calmes@univ-montp2.fr

[b] E. Wenger, Dr. C. Didierjean, Dr. E. Aubert
CRM2, UMR 7063 CNRS Université de Lorraine
Boulevard des Aiguillettes
54506 Vandoeuvre-lès-Nancy Cedex (France)

[c] Dr. M. C. Averlant-Petit
LCPM - UMR 7568 CNRS Université de Lorraine
1 rue Grandville, 54001 Nancy Cedex 1 (France)

[⁺] These authors contributed equally to this work.

Supporting information for this article is available on the WWW under http://dx.doi.org/10.1002/chem.201302829.

synthesis of oligoureas alternating BAC residues and β^3-homo-amino acid derivatives (i.e., 1:1 pattern) that should provide a new specific helix geometry with potentially distinctive spatial positioning of the functional side-chains constituting the key of biological activity.

Results and Discussion

Design and synthesis of mixed-oligoureas: We described a series of oligoureas alternating (S or R)-BAC and (S)-β^3-hAla and (S)-β^3-hPhe, converted into their corresponding N-(2-aminopropyl)carbamoyl (APC) and N-(2-amino-3-phenylpropyl)carbamoyl (APPC) units, respectively (Figure 1). Homochiral mixed oligomers **2–5** were synthesized by using all-S absolute configuration building blocks. As homo-oligoureas of both (S)-BAC and (S)-N-(2-aminoalkyl) carbamoyl residues form stable right-handed 2.5-helices with a θ_1 angle value locked to approximately +55°, it could be assumed that the blocked or favorable (+)-synclinal conformation about the C_α–C_β bond of these S motifs, should lead to a right-handed helical mixed oligomer. However, whereas ϕ and θ_2 torsional angles values are positive and negative (+81 and −109°, respectively) for BAC residues in (S)-BAC homo-oligoureas,[10] they are permuted (−100 and +85°, respectively) for (S)-N-(2-aminoalkyl)carbamoyl residues in oligoureas described by the group of Guichard.[7] This permutation resulted in reversed direction of the macrodipole

in these helices. Thus, in homochiral mixed systems, helical secondary structures could be expected with an alternating reverse hydrogen-bond network as in the case of oligoamides alternating β^2 and β^3-homo-amino acids.[2] However, regardless of the sign of the θ_1 angle, we also investigated other ϕ and θ_2 torsion angle value combinations by using alternating stereochemistry in mixed oligoureas. For that purpose, a series of mixed heterochiral oligoureas were synthesized alternating (R)-BAC motifs with (S)-β^3-N-(2-aminoalkyl)carbamoyl residues, that is, oligoureas **10–13**.

Oligoureas **2–5** and **10–13** (Figure 1) were synthesized in solution by stepwise assembly using a standard *tert*-butoxycarbonyl (Boc)/benzyl (Bzl) strategy (refer to the Supporting Information for full details). The succinimidyl carbamate (OSu) derivatives (S)-**6** or (R)-**6** (Boc-(S or R)-BAC-OSu), (S)-**7** and (S)-**8** (Boc-(S)-APC-OSu and Boc-(S)-APPC-OSu), precursors of oligoureas, were prepared from Boc-(S or R)-ABOC-OH, Boc-(S)-β^3-hAla-OH, and Boc-(S)-β^3-hPhe-OH, respectively.[10,12]

As previously reported for BAC homo-oligoureas,[10] N-benzhydryl-glycolamide ester (OBg ester) was introduced at the C-terminal part of the oligoureas as a β-Ala-OBg residue and a 4-bromophenyl group was introduced through its isocyanate derivative for capping the oligourea N-terminus.

The first coupling was performed by adding an equimolar amount of H-β-Ala-OBg to the activated monomer (S)-**6** (or (R)-**6**) in the presence of N,N-diisopropylethylamine (DIEA). Then, oligoureas **2–5** and **10–13** were prepared by

Activated monomeric blocks

Oligoureas with (S)-BAC
2 n = n' = n'' = 0
3 n = 1, n' = n'' = 0
4 n = n' = 1, n'' = 0
5 n = n' = n'' = 1
Oligoureas with (R)-BAC
10 n = n' = n'' = 0
11 n = 1, n' = n'' = 0
12 n = n' = 1, n'' = 0
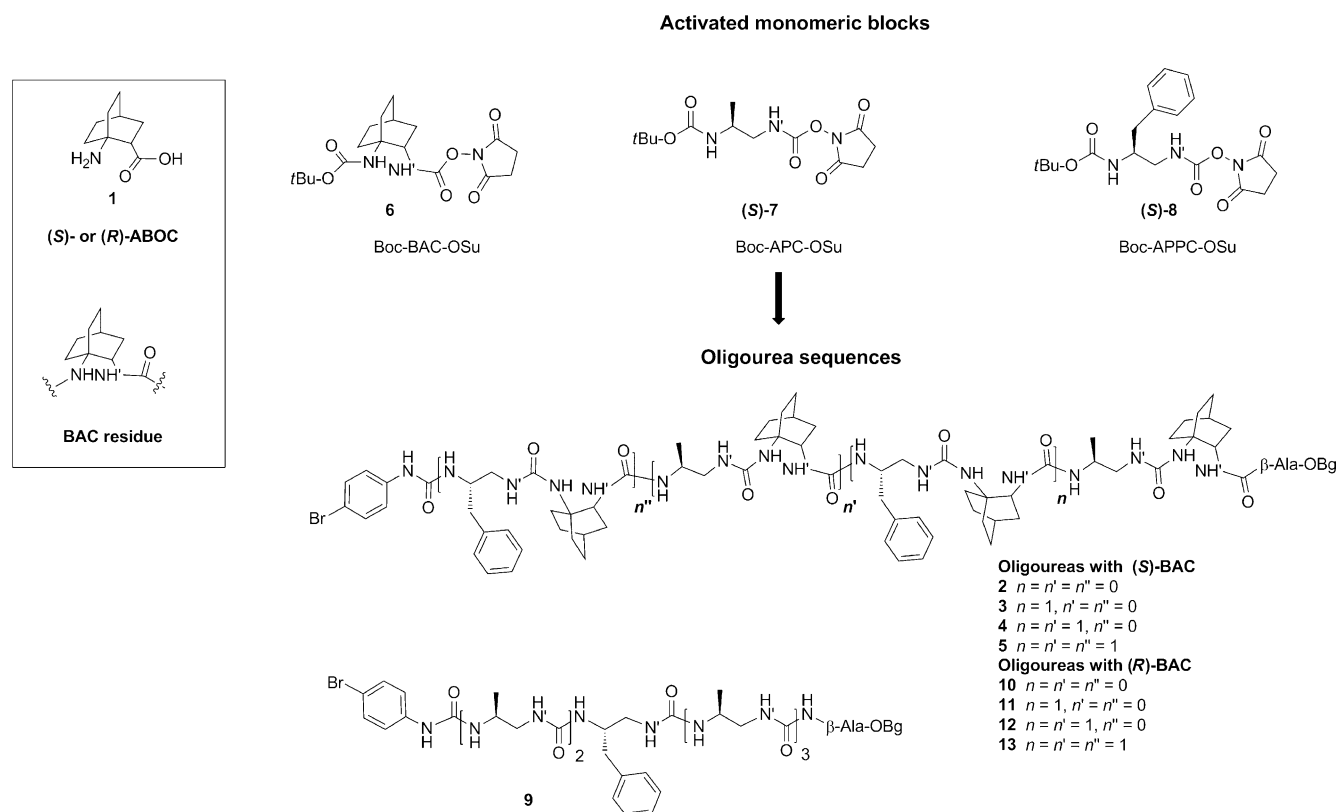**13** n = n' = n'' = 1

Figure 1. Oligoureas **2–5**, **10–13**, and **9** and monomeric blocks.

successive Boc deprotection, trifluoroacetic acid (TFA) salt neutralization and a coupling reaction using alternatively the three activated monomers (*S* or *R*)-**6** and (*S*)-**7/8** (refer to the Supporting Information for full details). After the last coupling and deprotection of the oligomers, one equivalent of 4-bromophenyl isocyanate was added for the final capping.

An oligourea containing (*S*)-APC acyclic residues (oligourea **9**), in place of the (*S*)-BAC residues in oligourea **4**, was also synthesized to emphasize the impact of the BAC motif. This oligourea was prepared according to the same procedure as that of oligoureas **2–5** and **10–13** in solution by stepwise assembly using Boc-(*S*)-APC-OSu and Boc-(*S*)-APPC-OSu (for details refer to the Supporting Information).

CD Spectroscopic analysis: First, to investigate the propensity of the oligoureas to fold, circular dichroism (CD) spectra were recorded in MeOH. In contrast to CD spectra of the (*S*)-BAC homo-oligoureas and the control oligoureas **9** that exhibited a strong maximum at 205.3 nm and to a less extent at 203.2 nm, respectively, those of the alternating sequences **2–5** did not display the helix oligourea characteristic CD signatures (Figure 2). Indeed, no signal increase was observed with the oligomer length and only a small maxi-

mum, left-shifted at about 200 nm, was observed for oligoureas **4** and **5**. This suggests that (*S*)-homochiral oligoureas did not adopt any particular folded helical structure in MeOH. In contrast to the homochiral oligomers **2–5**, the heterochiral (*R*)-BAC/(*S*)-APC/(*S*)-APPC oligoureas **10–13** displayed typical well-folded oligourea helix signature with a minimum around 204 nm indicating a left-handed rotation.

The per-urea molar ellipticity absolute value of this minimum increased with the number of monomers, indicating an increased stability as a function of the oligourea lengths. Interestingly, for tetra- and hexamer **11** and **12** and (*S*)-BAC homo-oligourea the intensities of the extrema share close absolute values (Figure 2).

Only the CD signature of the *R*/*S* dimer **10** had an extremum signal intensity significantly lower than that of the corresponding (*S*)-BAC-homo-dimer. These CD data highlighted that mixed oligoureas with four residues alternating only two constrained BAC residues had a similar ability to fold as the BAC homo-tetramer. This displays again the high propensity of BAC residue to induce folding even in mixed sequences, because a tetramer of acyclic residues did not show a typical profile of a folded structure in solution.[5] In addition, as previously observed for the (*S*)-BAC homo-oligoureas, the partially unfolded state that was induced by a rise in the temperature to 55 °C, suggested by the limited loss of signal, was also perfectly reversible for the mixed oligoureas **10–13** (the Supporting Information, Figure S1).

NMR analysis: NMR experiments were carried out in [D$_3$]methanol for all compounds and also in [D$_6$]DMSO for the *S*/*S* series and hexamers **9** and **12**. Proton assignments were obtained from a combined analysis of the COSY, TOCSY, and ROESY spectra. Nitrogen and carbon assignments were deduced from the ^{15}N HSQC and ^{13}C HSQC spectra, respectively. ^{13}C HSQC/TOCSY experiments were recorded to check the BAC methylene-group assignments (Tables S1–10, the Supporting Information).

Well-resolved spectra were obtained for both oligoureas **10–13** alternating (*R*)-BAC, (*S*)-APC, and (*S*)-APPC motifs (*R*/*S* series) and for compound **9**. On the contrary, (*S*)-BAC containing oligoureas **2–5** (*S*/*S* series) exhibited a very weak signal dispersion and broad line widths in CD$_3$OH (Figure 3 and the Supporting Information, Figure S4). Consequently, nearly all ^{1}H-, ^{15}N-, and ^{13}C NMR spectroscopic resonances were assigned for the *R*/*S* sequences (in CD$_3$OH and **12** in [D$_6$]DMSO), whereas the numerous signal overlaps in the (*S*/*S*)-oligoureas significantly complicated the chemical shift assignments and ^3J measurements in CD$_3$OH, even when a temperature of 323 K was permitted to globally improve the spectra quality. High-quality spectra were recovered in [D$_6$]DMSO, then nearly all resonances were assigned and ^3J values and $\Delta\delta$($^\alpha$CH) were accurately measurable in [D$_6$]DMSO for the entire *S*/*S* series.

Chemical shift differences between diastereotopic $^\alpha$CH protons and large ^3J(NH, $^\beta$CH) and ^3J(N'H, $^\alpha$CH) coupling constant values were previously described as useful evidences of a well-defined and stable acyclic oligourea secondary
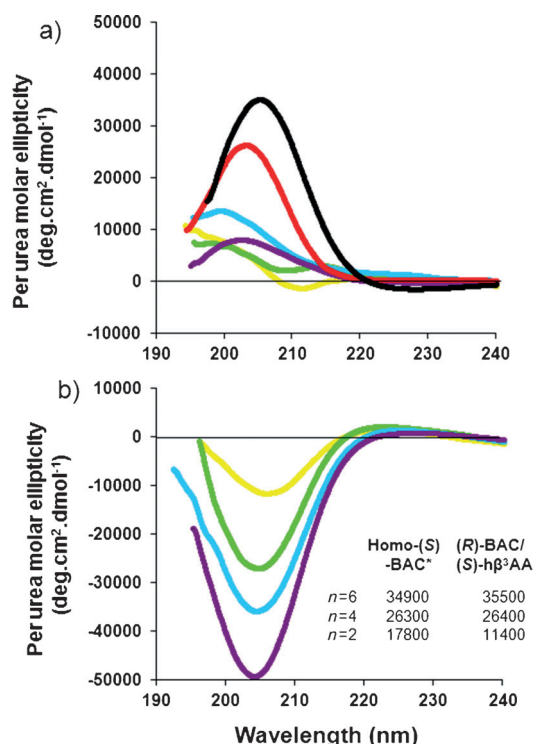

Figure 2. a) CD spectra of dimer **2** (yellow), tetramer **3** (green), hexamer **4** (cyan), and octamer **5** (purple) recorded at 20 °C in MeOH (200 μM). (*S*)-BAC homo-oligomer and control hexamer **9** profiles are shown in black and red, respectively; b) CD spectra of dimer **10** (yellow), tetramer **11** (green), hexamer **12** (cyan), and octamer **13** (purple) recorded at 20 °C in MeOH (200 μM). Comparison of extrema signal intensities of the (*S*)-BAC and mixed oligoureas.
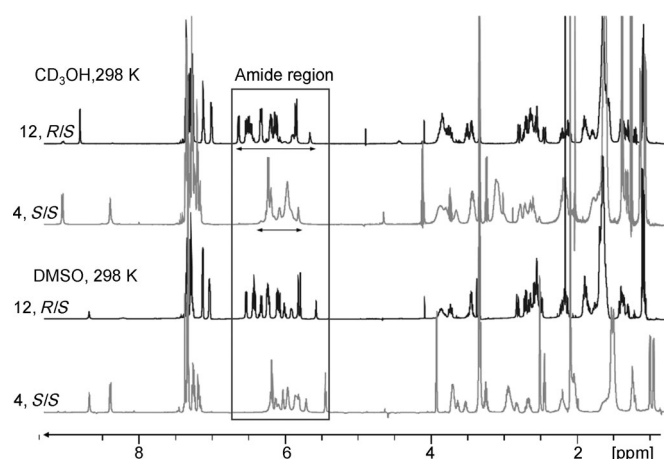
Figure 3. ^{1}H NMR spectra of compounds **4** and **12** (*S/R*- and *S/S* series, respectively) in CD$_3$OH and [D$_6$]DMSO at 298 K.

structures.[4] These features were observed for the control compound **9** (Tables S11–13, the Supporting Information). For (*R/S*)-oligoureas **10–13**, noticeable chemical shift differ-

ences $(0.57 < \Delta\delta(^\alpha CH) < 1.32$ ppm) were observed between the diastereotopic $^\alpha CH$ protons of the acyclic motifs. Moreover $^3J(NH, ^\beta CH)$, and $^3J(N'H, ^\alpha CH)$ coupling constant values were characteristic of an antiperiplanar arrangement between the NH and the $^\beta CH$ of the acyclic motif and the N'H and the $^\alpha CH$ of the BAC motif in CD$_3$OH (^3J average values ($^3J_{av}$) were (9.4 ± 0.6) Hz over the entire *R/S* series and (9.8 ± 0.2) Hz for compound **9**; Tables S13 A and B, the Supporting Information). The $^\alpha CH$ methylene pairs were all degenerated $(\Delta\delta(^\alpha CH) < 0.1$ ppm) for the (*S/S*)-oligoureas **2–5** in CD$_3$OH and [D$_6$]DMSO and ^3J values in [D$_6$]DMSO were typical of a random configuration, that is, $^3J_{av} = 7.5 \pm 0.1$ Hz for the *S/S* series (Tables S11 and S12, and Figure S13 B, the Supporting Information). Numerous cross-peaks were observed on the 2D ^{1}H ROESY spectra (Tables S14–18, the Supporting Information). Weak- and medium- $^\beta CH(i)/NH(i+2)$, $^\beta CH(i)/N'H(i+3)$, $^\alpha CH(i)/NH(i+2)$ (plain arrows), $^\beta CH(i)/^\xi CH(i+3)$ (dashed arrows) and $^\beta CH(i)/^\gamma CH(i+2)$ (dotted arrows) medium- and long-range NOE for oligoureas **10–13** were compatible with a 2.5-helix (Figure 4 b and the Supporting Information, Figure S5 and
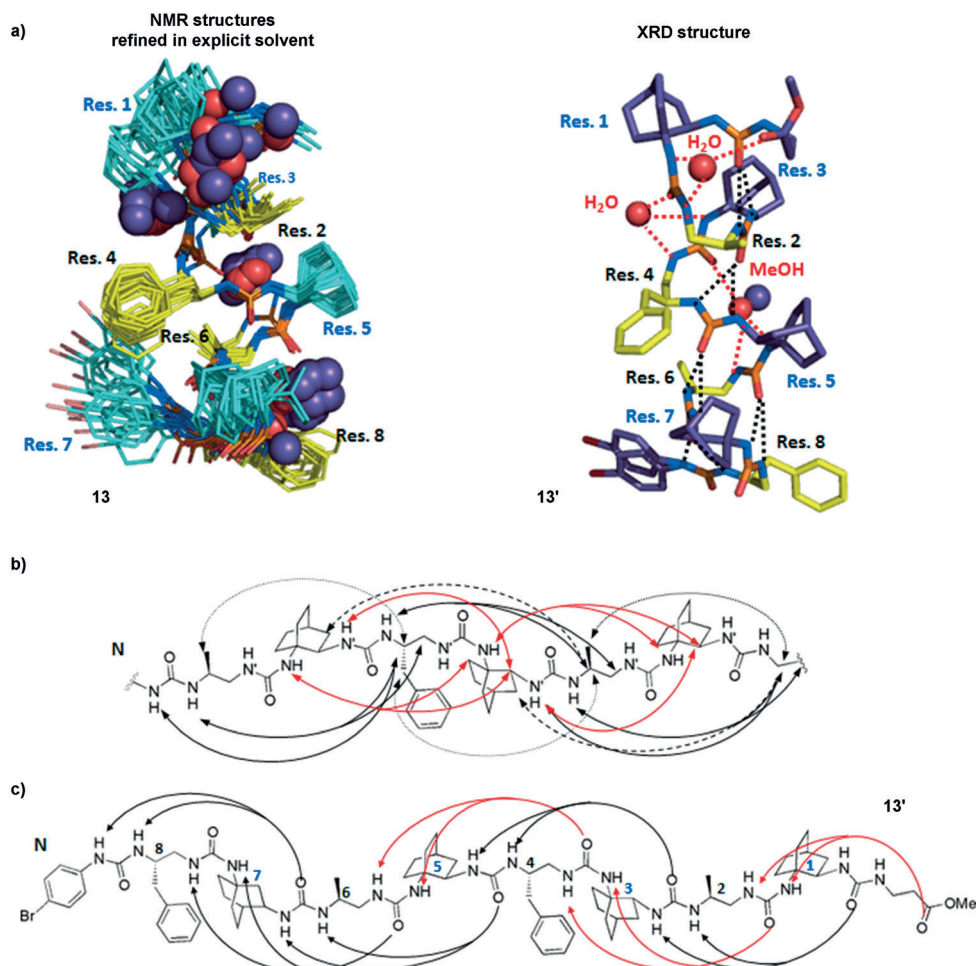

Figure 4. a) NMR solution structure of **13** refined in a methanol box and X-ray crystal structure (purple) of **13′**. Acyclic (*S*)-*N*-(2-aminoalkyl)carbamoyl are represented in yellow. Typical hydrogen-bonds are shown in dashed lines. The disordered C-terminal moiety and protons have been omitted for clarity; b) Characteristic long-range NOE correlations are in black. Putative NOE correlations of the non-solvated oligomer are in red; c) Typical hydrogen-bond networks observed in the crystal structure of **13′**. Hydrogen bonds mediated by solvent molecules are represented by red arrows.

Tables S15–18). However, it was noteworthy that the network of NOE was not regularly observed all along the urea system, because some recurrent long-range correlations were missing (in red arrows, Figure 4c). As expected, the oligourea **9** exhibited similar correlations of those previously described for this type of oligoureas that is, NH(i)/$^\beta$CH(i+2) and N(H(i)/$^\alpha$CH(i+2) (Figure S5 and Table S14, the Supporting Information).

Additionally, the time dependence of the amide proton-signal intensities in ^{1}H–^{2}D exchange in CD$_3$OD was studied (Figure 5 and Figure S8, the Supporting Information). The
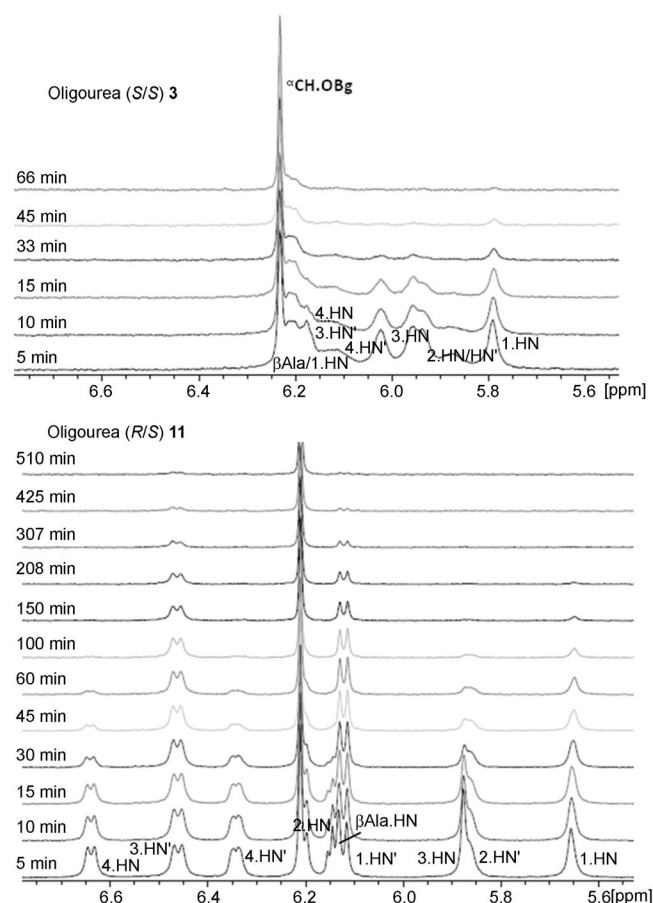

Figure 5. NH/ND exchange of urea protons in (S/S)-oligourea **3** and (S/R)-oligourea **11**.

results show that a rapid amide-proton exchange occurred in the S/S series, whereas a residual signal remained after several hours in the R/S series suggesting shielded and stable H-bonds in this series. The ^{1}H NMR spectrum of (S/S)-oligourea **3** exhibited broad line widths and the amide-proton resonances were not enough resolved to allow the accurate measurements of their intensities. Nevertheless, we could observe that the amide-proton signals quickly disappeared and after 100 min no signal could be detected. In contrast, for the corresponding (R/S)-oligourea **11**, we observed residual signals even after 500 min. The longer oli-

goureas show similar trends. These results showed that the S/S oligomers are significantly less-ordered than the hetero-oligomers.
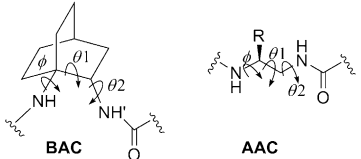
Overall, these results supported that the mixed (R/S)-oligoureas **10**–**13** might adopt preferential conformations, in contrast to the mixed (S/S)-oligoureas **2**–**5**. The latter underwent isomerization of urea bonds highlighted by strong N'H(i)/$^\alpha$CH(i+1) NOEs and may only display local and transient substructures according to the BAC residue rigidity.

Structural characterization: The typical structure of mixed heterochiral oligoureas was characterized both in solution and in the solid state (Figure 4). Thanks to the crystallization of the octamer **13′**, obtained by a partial transesterification of **13** during the long crystallization process in MeOH/water mixture (refer to the Supporting Information), a crystal structure of a mixed oligourea was obtained. The asymmetric unit contained one octamer molecule that adopted a left-handed 2.5-helix with a macrodipole from C- to N-terminus and a pitch around 5.1 Å. In the crystal, the molecules stacked into infinite columns in a head-to-tail manner as usually observed in solid state structures of helical foldamers like the poly-(S)-BAC oligourea (Figure S9, the Supporting Information). Among the two continuous bifurcated hydrogen-bond networks in the helix of **13′**, one network was mediated by three intercalated solvent molecules, which acted as bridges between the urea NH and the carbonyl groups (Figure 4). In (S)-BAC-homo-oligoureas[10] and oligoureas derived from (S)-β^3-homo-amino acids,[6] intercalation of a solvent molecule when observed, disrupted only the first hydrogen-bond of the helix. In octamer **13′**, the hydrogen bonds involving the first, third, and fifth urea linkages were perturbed by either water or methanol molecules. It was noteworthy that **13′** solid-state structure was compatible with the disrupted characteristic (R/S)-oligoureas set of NOE, pointing out the presence of highly populated solvated oligomers in solution. In this context, the elucidation of the NMR structure of **13** was performed by using classical protocols of molecular modeling calculations in vacuum, followed by a refinement step in explicit methanol solvent using AMBER 10[13] (Table S19 and Figures S6 and S7, the Supporting Information). Refined NMR structure calculations showed the ability of the octamer **13** to incorporate solvent molecules into the same hydrogen-bond network than that observed within the crystal (Figure 4a). Preferential localizations of the solvent molecule intercalations were further investigated by density functional theory (DFT) calculations. Bond interaction energies estimated from these theoretical calculations[14] were nearly equivalent for the two hydrogen-bond networks of the optimized helix (Figure S10, the Supporting Information). On the other hand, this study showed that the stiffness of the deformation around the ϕ dihedral angle was larger in the BAC residue compared with the acyclic residue (Figure S11 and S12). Thus, the conformational freedom of APC2, APPC4 residues, and the terminal ester allowed the opening of the helix groove to catch solvent molecules according to NMR and crystal data. All

the results showed that mixed oligoureas **10–13** exhibited a similar 2.5-helix compared with the poly-(*S*)-BAC oligourea series, with a reverse helical handedness driven by the configuration of the BAC residue.

Backbone torsional angle analysis: The typical ϕ, θ_1, and θ_2 torsion angles of each monomer type in mixed oligoureas **10–13** were measured and compared to those previously obtained for (*S*)-BAC-homo-oligourea[10] and for the acyclic oligoureas[6] (Table 1 and the Supporting Information,

Table 1. Characteristic torsional angles of the oligoureas.

Motifs	Angle values [°]	Poly-(*S*)-BAC[10]	Acyclic oligoureas[6]	13 (NMR)[a], 13′ (XRD)[b,c]
BAC	ϕ	81 ± 14		-70 ± 9
	$(\phi)^{[b]}$	63 ± 6		$-67 \pm 4^{[b]}$
	θ_1	51 ± 6		-52 ± 4
	$(\theta_1)^{[b]}$	54 ± 9		$-61 \pm 3^{[b]}$
	θ_2	-102 ± 13		104 ± 14
	$(\theta_2)^{[b]}$	-109 ± 21		103 ± 4^{b}
AAC	ϕ		-100	-122 ± 26
	$(\phi)^{[b]}$		-103	-101 ± 34
	θ_1		43	-57 ± 6
	$(\theta_1)^{[b]}$		57	-56 ± 4
	θ_2		96	104 ± 9
	$(\theta_2)^{[b]}$		80	111 ± 8

[a] Angle value in the NMR structure refined in explicit CD$_3$OH solvent. [b] Angle value in the crystal structure. [c] ϕ Angle value of the C-terminal BAC residues was omitted.

Table S21). According to their highly restrained conformational freedom, not only the θ_1 but all torsion angles values of the (*R*)-BAC residues in **10–13**, compared to those observed in the poly-(*S*)-BAC solution and solid-state structures,[10] were remarkably conserved (Table 1 and Table S21, the Supporting Information).

However, considering the configuration of the BAC residue, the signs of the angle values were inverted. On the other side, the (*S*)-*N*-(2-aminoalkyl)carbamoyl motifs (AAC motifs) underwent significant conformational rearrangement compared to the acyclic oligoureas. Whereas both ϕ and θ_2 dihedral angles signs and values were similar, the gauche dihedral angle θ_1 of the AAC motifs was of reverse sign in the heterochiral mixed oligourea series. The resulting (−)-synclinal conformation around the C$_\alpha$−C$_\beta$ bond, although sterically less favorable than the (+)-synclinal conformation taking into account the side-chain substituent R,[2] was imposed by the (*R*)-BAC residue leading to homogeneous torsion angle values through the different motifs all along the edifice. It is noteworthy that during the submission process of this article, the effect on the folding or misfolding of the stereochemistry of a cyclic unit (cyclohexyl unit) inserted at the central position of an oligourea has been reported.[15] Albeit

limited to one cyclic residue in the sequence, this study showed that the cyclohexyl derivative closely match the torsion angles of the acyclic residues in the 2.5-helix and that, in contrast to the BAC residue, did not impact on the conformation of the adjacent canonical residue.

Overall, these results highlight the strong ability of the BAC residue to drive helical folding in the heterochiral compounds **10–13**. However it failed to induce a helical structure in the homochiral series.

Subunit configuration impact on the folding or misfolding: On the basis of a typical left-handed 2.5-helix oligourea structure (Figure 6) a plausible explanation on the misfolding of the *S/S* series could be proposed. In this model, that is, (*S*)-BAC/*N*-(2-aminoethyl)carbamoyl alternations, it appeared that pro-*S* and pro-*R* protons of the *N*-(2-aminoethyl)carbamoyl motifs were in an ″intermediate″ position (about 45° relative to the axis of the helix) between the axial and lateral one commonly observed in amino acid-based foldamers.[2] In the case of homochiral oligoureas, the i residue side-chain at the pro-*S* position would be in the direct proximity (ca. 2.8 Å) of the adjacent bifurcated hydrogen bond CO(i)···NH(i+1)/NH′(i+2). By preventing formation of this bifurcated hydrogen bond, the whole edifice would not be able to fold. In contrast, in the heterochiral oligourea, the more favorable distance between an amino acid side-chain in the pro-*R* position and the bifurcated hydrogen-bond allowed the folding.
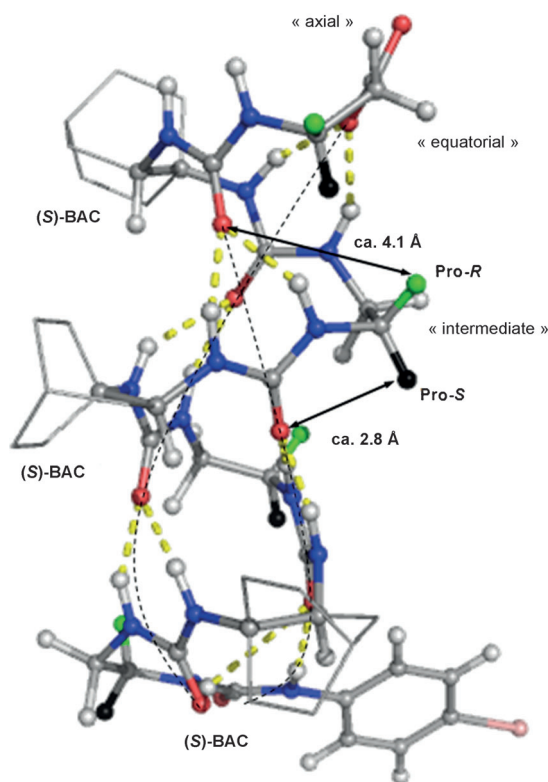

Figure 6. Schematic representation to explain the misfolding of the *S/S* series.

Conclusion

We have designed a mixed and stable left-handed 2.5-helix alternating the BAC motif and acyclic β³-homo-amino acid derivatives linked through a urea linkage. The benefits brought by the strongly restrained BAC motif, already observed in poly-(S)-BAC oligoureas, were conserved in mixed sequences, that is, stability, high helical propensity and no isomerization of the urea bond. These mixed systems highlighted the particularly interesting properties of the BAC motif as a helix inducer since it has the ability to impose an unfavorable conformation around the C_α–C_β bond of the adjacent (S)-N-(2-aminoalkyl)carbamoyl moiety. Moreover, in these mixed-oligourea systems, the crucial arrangement of the side chain of the β³-homo-amino acid derivatives along the helix surface could be predicted. Thus, these oligomers provide particularly attractive molecular architecture and represent solid bases to go further into the design of stable and functionalized secondary structures usable as biological tools, in particular for the design of protein–protein interaction modulators.

Experimental Section

General procedures: All reagents were used as purchased from commercial suppliers without further purification. Solvents were dried and purified by conventional methods prior to use. Melting points were determined with a Büchi 510 Melting Point. Optical rotations were measured with a Perkin–Elmer 341 polarimeter. ^{1}H or ^{13}C NMR spectra (DEPT, ^{1}H/^{13}C 2D-correlations) were recorded with Bruker A DRX 400 and 600 spectrometers using the solvent as internal reference. Data are reported as follows: chemical shifts (δ) in parts per million, coupling constants (J) in hertz (Hz). The ESI mass spectra were recorded with a platform II quadrupole mass spectrometer (Micromass, Manchester, UK) fitted with an electrospray source. RP-HPLC analyses were performed with a Waters model 510 instrument with variable detector using column A: Chromolith SpeedROD RP-18e, 2μ, (50×4.6 mm), flow: 3 mL min^{-1}, H$_2$O (0.1% TFA)/CH$_3$CN (0.1% TFA), gradient 0→100% (4 min) and 100% (1 min).

The enantiopure compounds (S)- and (R)-aminobicyclo[2.2.2]octane-2-carboxylic acid (S)-**1** and (R)-**1** and (S)- and (R)-1-tert-butyloxycarbonylaminobicyclo[2.2.2]octane-2-carboxylic acid (Boc-(S)-ABOC-OH and Boc-(R)-ABOC-OH) were prepared as previously described.[16]

General procedure for the preparation of O-succinimidyl-2-(tert-butyloxycarbonyl amino)carbamates (S)-6, (S)-7 and (S)-8: N-methylmorpholine (1.1 equiv) and ethylchloroformate (1.1 equiv) were added to a solution of Boc-(S)-β-amino acid (1.0 equiv) in dry THF (15 mL) under an argon atmosphere at −20 °C. The solution was stirred at −20 °C for 20 min and the resulting white suspension was allowed to warm to −5 °C. Then, an aqueous solution (2 mL) of sodium azide (2.5 equiv) was added dropwise and the solution was stirred at the same temperature for 5 min. The reaction mixture was diluted with toluene (20 mL), washed with brine, dried over MgSO$_4$ and partially concentrated in vacuo to a 0.1 M solution of the corresponding acyl azide. This solution was heated to 65 °C with stirring and under an argon atmosphere for 10 min. After observing gas evolution, N-methylmorpholine (1.0 equiv) and N-hydroxysuccinimide (0.95 equiv) were added. The mixture was stirred at the same temperature for 10 min and then cooled to room temperature. The solvent was removed in vacuo and the residue triturated with diethyl ether to yield the title compound collected by filtration.

(S)-O-Succinimidyl-2-(tert-butoxycarbonylamino)bicyclo-[2.2.2]octanylcarbamate (S)-6: Synthesized according to the general procedure from (S)-1-tert-butyloxycarbonylamino bicyclo[2.2.2]octane-2-carboxylic acid (Boc-(S)-ABOC-OH) (1.08 g, 1 equiv, 4.0 mmol). The crude expected compound (S)-**6** was obtained as a white solid (1.21 g, 3.17 mmol, 79%) and was used without further purification in the following step. M.p. 145 °C; $[\alpha]_D^{20} = +26$ (c = 1.0 in CH$_2$Cl$_2$); ^{1}H NMR (400 MHz, CDCl$_3$, 25 °C): δ = 1.40 (m, 9H, C(CH$_3$)$_3$), 1.55 (m, 1H, HCH), 1.60–1.70 (m, 6H, 2CH$_2$ and HCH), 1.72–1.82 (m, 2H, CH$_2$), 2.15–2.22 (m, 2H, CH$_2$), 2.78 (s, 4H, CH$_2$CO), 3.94 (br s, 1H, 2-H), 4.55 (s, 1H, NH), 6.84 ppm (br s, 1H, NH); ^{13}C NMR (100 MHz, CDCl$_3$, 25 °C) 24.0 (4-C), 24.7 (CH$_2$), 24.8 (CH$_2$CO), 25.4 (C(CH$_3$)$_3$), 28.3 (CH$_2$), 35.9 (CH$_2$), 52.2 (2-C), 65.8 (1-C), 79.9 (C(CH$_3$)$_3$), 151.6, 155.6, 169.9 ppm (CO); MS (ESI) m/z: 282.1 [(M+H−Boc)$^+$], 382.2 [M+H$^+$]; HRMS (ESI): m/z calcd for C$_{14}$H$_{24}$N$_9$O$_4$: 382.1951 [M+H$^+$]; found: 382.1972.

(S)-O-Succinimidyl-2-(tert-butyloxycarbonylamino)-propylcarbamate (S)-7: Synthesized according to the general procedure from Boc-β³-hAla-OH (1.0 g, 4.9 mmol, 1.0 equiv). The crude expected compound (S)-**7** was obtained as a white solid and (1.18 g, 3.7 mmol, 76%) was used without further purification in the following step. R_t (HPLC) column A = 1.32 min; ^{1}H NMR and ^{13}C NMR data are identical to those previously described.[17] MS (ESI): m/z: 216.1 [(M+H−Boc)$^+$], 316.1 [M+H$^+$], 338.0- [M+Na$^+$], 631.1[2M+H$^+$].

(S)-O-Succinimidyl-2-(tert-butyloxycarbonylamino)-4-phenylpropylcarbamate (S)-8: Synthesized according to the general procedure from Boc-β³-hPhe-OH (1.0 g, 3.6 mmol, 1.0 equiv). The crude expected compound (S)-**8** was obtained as a white solid (1.11 g, 2.8 mmol, 79%) and was used without further purification in the following step. R_t (HPLC) column A = 2.30 min; ^{1}H NMR and ^{13}C NMR data are identical to those previously described.[17] MS (ESI): m/z: 292.4 [(M+H−Boc)$^+$], 392.4 [M+H$^+$], 414.4[M+Na$^+$]

(R)-O-Succinimidyl-2-(tert-butoxycarbonylamino)bicyclo-[2.2.2]octanylcarbamate (R)-6: Synthesized according to the general procedure from (R)-1-tert-butyloxycarbonylamino bicyclo[2.2.2]octane-2-carboxylic acid (Boc-(R)-ABOC-OH). $[\alpha]_D^{20} = -26$ (c = 1.0 in CH$_2$Cl$_2$); MS and NMR data are identical to those of the (S)-enantiomer.

Boc-β-Ala-OBg: The N-Benzhydryl-glycolamide (OBg) ester of Boc-β-Ala-OH (Boc-β-Ala-OBg) was obtained by esterification with N-benzhydryl-bromoacetamide in the presence of 1,8-diazabicyclo[5,4,0]undec-7-ene (DBU) as previously described[18] under microwave irradiation (15 min at 100 °C). M.p. 86 °C; t_R (HPLC, column A) = 2.41 min; ^{1}H NMR (400 MHz, CDCl$_3$, 25 °C): δ = 1.39 (s, 9H, C(CH$_3$)$_3$), 2.59 (t, J = 8.0 Hz, 2H, CH$_2$-CO), 3.40 (m, 2H, NH-CH$_2$), 4.63 (s, 2H, OCH$_2$), 5.01 (br.s, 1H, NH), 6.32 (d, J = 8.0 Hz, 2H, CH), 7.03 (br.s, 1H, NH), 7.24–7.35 ppm (m, 10H, H-arom); ^{13}C NMR (100 MHz, CDCl$_3$, 25 °C): δ = 28.3 (C(CH$_3$)$_3$), 35.0 (CH$_2$), 36.2 (CH$_2$), 56.6 (CH), 63.3 (CH$_2$), 79.7 (C), 127.4, 127.6, 128.7 (CH-arom), 141.0 (C-arom), 155.9, 166.1, 171.0 ppm (CO); MS (ESI) m/z: 313.1 [(M+H−Boc)$^+$], 413.1 [M+H$^+$], 435.1[M+Na$^+$]; HRMS (ESI): m/z calcd for C$_{23}$H$_{29}$N$_2$O$_5$: 413.2076 [M+H$^+$]; found: 413.2077.

General procedure for the preparation of oligoureas 2–5, 9, and 10–13: For full details refer to the Supporting Information.

Deprotection: TFA (3 mL) was added to a solution of the Boc-β-Ala-OBg or N-Boc-protected intermediate urea (1.0 equiv) in CH$_2$Cl$_2$ (7 mL) (0.1 M) and the mixture was stirred for 1 hour until completion of the reaction (monitored by HPLC, column A). The organic solvent and the excess of TFA were removed in vacuo and the crude product was diluted with ethyl acetate and was washed with a 1 M solution of NaHCO$_3$, dried over MgSO$_4$ and concentrated in vacuo. The di-, tetra-, hexa-, and octamer were purified by using preparative RP-HPLC for bromophenylisocyanate coupling. The other intermediates were used without further purification in the following succinimidyl carbamate coupling step.

Coupling step: Diisopropylethylamine (DIEA, Hünig's base) and (3.0 equiv) succinimidyl carbamate (S)-**6**, (R)-**6**, (S)-**7**, or (S)-**8** (1 equiv) were successively added to the free corresponding amine (white solid) in DMF (0.1 M). The reaction mixture was stirred at room temperature for 16 h and then was concentrated in vacuo. The residue diluted with ethyl acetate was successively washed with 1 N KHSO$_4$, brine, 1 N NaHCO$_3$,

brine, dried over $MgSO_4$ and concentrated in vacuo to yield the expected crude new intermediate compound that was used without further purification in the following step. HPLC and LC/MS analyses were used to characterize the compound.

Bromophenylisocyanate coupling: DIEA (3.0 equiv) was added to the pure TFA salt intermediate (di-, tetra, hexa-, and octamer) in DMF (0.1 M), which was followed, after stirring 10 min at room temperature, by the addition of bromophenylisocyanate (1.0 equiv). The reaction mixture was stirred at room temperature for 2 h and then was concentrated in vacuo. The residue was diluted with ethyl acetate and the precipitate formed was isolated by filtration to yield the expected oligoureas.

Circular dichroism: CD experiments were carried out using a Jasco J815 spectropolarimeter. The spectra were obtained in MeOH using a 1 mm path length CD cuvette, at 20–55 °C, over a wavelength range of 190–260 nm. Continuous scanning mode was used, with a response of 1.0 s with 0.2 nm steps and a bandwidth of 2 nm. The signal-to-noise ratio was improved by acquiring each spectrum over an average of two scans. The baseline was corrected by subtracting the background from the sample spectrum. The samples were dissolved in a spectrophotometric grade MeOH at 100–200 μm (Figure 2, S1 and S2, the Supporting Information).

NMR experiments: The NMR samples contained 5–10 mM of **2**–**5** and **9**–**13** dissolved in CD_3OH or/and $[D_6]DMSO$. All spectra were recorded on a Bruker Avance 600 AVANCE III spectrometer equipped with a 5 mm triple-resonance cryoprobe (^1H, ^{13}C, ^{15}N). Homonuclear 2D spectra DQF/COSY, TOCSY (DIPSI2), and ROESY were typically recorded in the phase-sensitive mode using the States-TPPI method as data matrices of 256–700 real (t_1) × 2048 (t_2) complex data points; 8–64 scans per t_1 increment with 1.0–1.5 s recovery delay and spectral width of 6009 Hz in both dimensions were used. The mixing times were 60 ms for TOCSY and 450 ms for the ROESY experiments. In addition, 2D heteronuclear spectra ^{15}N-, ^{13}C HSQC and ^{13}C HSQC-TOCSY were acquired to fully assign the ABOC residue (8–32 scans, 256–512 real (t_1) × 2048 (t_2) complex data points). Spectra were processed with Topspin (Bruker Biospin) and visualized with Topspin or NMRView on a Linux station. The matrices were zero-filled to 1024 (t_1) x 2048 (t_2) points after apodization by shifted sine-square multiplication and linear prediction in the F1 domain. Chemical shifts were referenced to TMS (Figure 3, S3, S4, S5 and S8, Tables S1–4, S5–8, S9, S10, S11, S12, S13 A and B, the Supporting Information).

Structure calculations: ^1H, ^{15}N, and ^{13}C chemical shifts were assigned according to classical procedures. NOE cross-peaks were integrated and assigned within the NMRView software.[19] The volumes of NOE peaks between methylene pair protons were used as reference of 1.8 Å. The lower bound for all restraints was fixed at 1.8 Å and upper bounds at 2.7, 3.3, and 5.0 Å, for strong, medium, and weak correlations, respectively. Pseudo-atoms corrections of the upper bounds were applied for unresolved aromatic, methylene and methyl protons signals as described previously.[20] Structure calculations were performed with AMBER 10[21] in two stages: cooking, simulated annealing in vacuum. The cooking stage was performed at 1000 K to generate 100 initial random structures. SA calculations were carried during 20 ps (20000 steps, 1 fs long) as described elsewhere. First, the temperature was risen quickly and was maintained at 1000 K for the first 5000 steps, then the system was cooled gradually from 1000 K to 100 K from step 5001 to 18000 and finally the temperature was brought to 0 K during the 2000 remaining steps. For the 3000 first steps, the force constant of the distance restraints was increased gradually from 2.0 to 20 kcal mol^{-1} Å. For the rest of the simulation (step 3001 to 20000), the force constant was kept at 20 kcal mol^{-1} Å. The 20 lowest-energy structures with no violations > 0.3 Å were considered as representative of the compound structure. The representation and quantitative analysis were carried out using Ptraj, MOLMOL[22] and PyMOL (Delano Scientific; Figure 4, Figures S5, S6, and S7 the Supporting Information, and Tables 1, S14–18, S19, and S21, the Supporting Information).

Refinement in explicit methanol solvent: The ability of the oligourea **13′** to incorporate solvent molecules was shown using a typical short refinement step based on those on the AMBER-based portal server for NMR structures.[18] The 20 representative structures calculated in vacuum were immersed in a methanol box with a layer of 10 Å. The refinement procedure includes the following steps: 1) minimization of the position of the methanol molecules keeping the solute fixed; 2) minimization of the entire systems; 3) the system was allowed to heat up from 0 to 300 K using weak restraints during 10 ps; 4) molecular dynamics using NMR distance restraints stage during 200 ps (time step of 0.2 fs) at 300 K and a constant pressure of 1 atm; 5) the system was then cooled to 0 K during 10 ps before 6) a final minimization stage (Figure 4, Table S21, the Supporting Information).

NH/ND exchange experiments in CD_3OD: Amide H/D exchange experiments were recorded at 293 K (pH*=7.8) immediately after dissolving the compounds **4**, **9**, and **13** in CD_3OD. NMR ^1H spectra were typically recorded after periods of approximately 5, 10, 15, 30, 45, 100, 150, 200, 300, 400, and 500 min. pH* corresponds to the apparent pH in methanol using the hydrogen electrode.[23]

Crystallographic data: Crystals for compound **13′** exhibited weak diffracting power. Their X-ray data were collected at 100 K with an Oxford Diffraction SuperNova diffractometer equipped with a copper microsource (λ=1.5418 Å). Diffraction data were processed using CrysAlis RED (Oxford Diffraction, 2012). An empirical absorption correction (μ= 12.5 cm^{-1}) was applied to all observed reflections. The structure was solved by direct methods with SIR2004[24] and the crystallographic refinements were conducted using SHELXL-97.[25] In the refinement, the terminal bromophenyl group was found to be disordered over two sites, with occupancies refined to 0.537(4) and 0.463(4). Selected crystallographic data are provided in Table S20 (the Supporting Information). CCDC-915829 (**13′**) contains the supplementary crystallographic data for this paper. These data can be obtained free of charge from The Cambridge Crystallographic Data Centre via www.ccdc.cam.ac.uk/data_request/cif.

DFT calculations: *Gas-phase calculations*: The molecular structure of octamer **13′** was optimized at the density functional level of theory using the Gaussian 09 software,[26] starting from the experimental X-ray structure of the helix (Figure S10, the Supporting Information). To reduce the computational cost, the bromophenyl group was substituted by a hydrogen atom. Solvent atoms from water and methanol molecules were removed prior to optimization. The B3LYP functional[27] was used together with the 6-31G(d,p) basis set. Non-explicit solvent interactions were modeled using a polarizable continuum model (PCM) model (solvent= methanol), and frequency calculation was performed to check that an energy minima was obtained at the end of the optimization procedure.

The strength of the hydrogen-bond networks in the helix was estimated using a topological analysis performed on the calculated electron density.[28] As shown in previous works,[29] the potential energy density at the bond critical point (V_{cp}) linking H and O atoms correlates with the H···O bond-dissociation energy ($E_{int} = 1/2 V_{cp}$). By using this relationship and the V_{cp} values obtained from the topological analysis, one obtains interaction energies for the two hydrogen-bond networks that are very close to each other: 143 and 126 kJ mol^{-1}, for even and odd links, respectively.

The stiffness of the torsion around the ϕ dihedral angle in BAC and APC residues was determined by relaxed potential-energy scans on model molecules using the Gaussian 09 software package (Figure S11, the Supporting Information). The B3LYP functional was used together with the 6-311G(d,p) basis set and no solvent effects were taken into account. The resulting energy profiles (Figure S12, the Supporting Information) show that the deformation around ϕ dihedral angle is much easier for APC-like molecule than for BAC-like molecule (Table S21, the Supporting Information). This is then certainly the reason why solvent water and methanol molecules insert only between residues that are linked by an APC-like residue.

[1] S. H. Gellman, *Acc. Chem. Res.* **1998**, *31*, 173–180; S. Hanessian, X. H. Luo, R. Schaum, S. Michnick, *J. Am. Chem. Soc.* **1998**, *120*, 8569–8570; D. J. Hill, M. J. Mio, R. B. Prince, T. S. Hughes, J. S. Moore, *Chem. Rev.* **2001**, *101*, 3893–4011; R. P. Cheng, S. H. Gellman, W. F. DeGrado, *Chem. Rev.* **2001**, *101*, 3219–3232; C. M. Goodman, S. Choi, S. Shandler, W. F. DeGrado, *Nat. Chem. Biol.* **2007**, *3*, 252–262; F. Bouillère, S. Thetiot-Laurent, C. Kouklovsky, V. Alezra, *Amino Acids* **2011**, *41*, 687–707; T. A. Martinek, F. Fulop, *Chem. Soc. Rev.* **2012**, *41*, 687–702.

[2] D. Seebach, A. K. Beck, D. J. Bierbaum, *Chem. Biodiversity* **2004**, *1*, 1111–1239.

[3] S. De Pol, C. Zorn, C. D. Klein, O. Zerbe, O. Reiser, *Angew. Chem.* **2004**, *116*, 517–520; *Angew. Chem. Int. Ed.* **2004**, *43*, 511–514; A. Hayen, M. A. Schmitt, F. N. Ngassa, K. A. Thomasson, S. H. Gellman, *Angew. Chem.* **2004**, *116*, 511–516; *Angew. Chem. Int. Ed.* **2004**, *43*, 505–510; G. V. M. Sharma, P. Nagendar, P. Jayaprakash, P. R. Krishna, K. V. S. Ramakrishna, A. C. Kunwar, *Angew. Chem.* **2005**, *117*, 6028–6032; *Angew. Chem. Int. Ed.* **2005**, *44*, 5878–5882; G. Srinivasulu, S. K. Kumar, G. V. M. Sharma, A. C. Kunwar, *J. Org. Chem.* **2006**, *71*, 8395–8400; D. Seebach, B. Jaun, R. Sebesta, R. I. Mathad, O. Flogel, M. Limbach, H. Sellner, S. Cottens, *Helv. Chim. Acta* **2006**, *89*, 1801–1825; W. S. Horne, S. H. Gellman, *Acc. Chem. Res.* **2008**, *41*, 1399–1408; P. G. Vasudev, S. Chatterjee, N. Shamala, P. Balaram, *Chem. Rev.* **2011**, *111*, 657–687; L. K. A. Pilsl, O. Reiser, *Amino Acids* **2011**, *41*, 709–718; T. A. Martinek, I. M. Mándity, L. Fulop, G. K. Toth, E. Vass, M. Hollosi, E. Forro, F. Fulop, *J. Am. Chem. Soc.* **2006**, *128*, 13539–13544; I. M. Mándity, E. Weber, T. A. Martinek, G. Olajos, G. K. Toth, E. Vass, F. Fulop, *Angew. Chem.* **2009**, *121*, 2205–2209; *Angew. Chem. Int. Ed.* **2009**, *48*, 2171–2175; I. M. Mándity, L. Fulop, E. Vass, G. K. Toth, T. A. Martinek, F. Fulop, *Org. Lett.* **2010**, *12*, 5584–5587.

[4] V. Semetey, D. Rognan, C. Hemmerlin, R. Graff, J. P. Briand, M. Marraud, G. Guichard, *Angew. Chem.* **2002**, *114*, 1973–1975; *Angew. Chem. Int. Ed.* **2002**, *41*, 1893–1895.

[5] A. Violette, M. C. Averlant-Petit, V. Semetey, C. Hemmerlin, R. Casimir, R. Graff, M. Marraud, J. P. Briand, D. Rognan, G. Guichard, *J. Am. Chem. Soc.* **2005**, *127*, 2156–2164.

[6] L. Fischer, P. Claudon, N. Pendem, E. Miclet, C. Didierjean, E. Ennifar, G. Guichard, *Angew. Chem.* **2010**, *122*, 1085–1088; *Angew. Chem. Int. Ed.* **2009**, *49*, 1067–1070.

[7] L. Fischer, G. Guichard, *Org. Biomol. Chem.* **2010**, *8*, 3101–3117.

[8] J. Fremaux, L. Fischer, T. Arbogast, B. Kauffmann, G. Guichard, *Angew. Chem.* **2011**, *123*, 11584–11587; *Angew. Chem. Int. Ed.* **2011**, *50*, 11382–11385.

[9] C. André, B. Legrand, C. Deng, C. Didierjean, G. Pickaert, J. Martinez, M. C. Averlant-Petit, M. Amblard, M. Calmes, *Org. Lett.* **2012**, *14*, 960–963.

[10] B. Legrand, C. André, E. Wenger, C. Didierjean, M. Averlant-Petit, J. Martinez, M. Calmès, M. Amblard, *Angew. Chem. Int. Ed.* **2012**, *51*, 11267–11270.

[11] For a recent review, see: V. Azzarito, K. Long, N. S. Murphy, A. J. Wilson, *Nat. Chem.* **2013**, *5*, 161–173.

[12] V. Semetey, C. Hemmerlin, C. Didierjean, A. P. Schaffner, A. G. Giner, A. Aubry, J. P. Briand, M. Marraud, G. Guichard, *Org. Lett.* **2001**, *3*, 3843–3846.

[13] D. A. Case, T. A. Darden, T. E. Cheatham III, C. L. Simmerling, J. Wang, R. E. Duke, R. Luo, M. Crowley, R. C. Walker, W. Zhang, K. M. Merz, B. Wang, S. Hayik, A. Roitberg, G. Seabra, I. Kolossváry, K. F. Wong, Paesani. F., J. Vanicek, X. Wu, S. R. Brozell, T. Steinbrecher, H. Gohlke, L. Yang, C. Tan, J. Mongan, V. Hornak, G. Cui, D. H. Mathews, M. G. Seetin, C. Sagui, V. Babin, P. A. Kollman, *AMBER 10, University of California, San Francisco.* **2008**; V. Hornak, R. Abel, A. Okur, B. Strockbine, A. Roitberg, C. Simmerling, *Proteins Struct. Funct. Bioinf.* **2006**, *65*, 712–725.

[14] M. E. Brezgunova, E. Aubert, S. Dahaoui, P. Fertey, S. Lebegue, C. Jelsch, J. G. Angyan, E. Espinosa, *Cryst. Growth Des.* **2012**, *12*, 5373–5386.

[15] N. Pendem, C. Douat, P. Claudon, M. Laguerre, S. Castano, B. Desbat, D. Cavagnat, E. Ennifar, B. Kauffmann, G. Guichard, *J. Am. Chem. Soc.* **2013**, *135*, 4884–4892.

[16] O. Songis, C. Didierjean, C. Laurent, J. Martinez, M. Calmes, *Eur. J. Org. Chem.* **2007**, 3166–3172.

[17] G. Guichard, V. Semetey, C. Didierjean, A. Aubry, J. P. Briand, M. Rodriguez, *J. Org. Chem.* **1999**, *64*, 8702–8705.

[18] I. Bertini, D. A. Case, L. Ferella, A. Giachetti, A. Rosato, *Bioinformatics* **2011**, *27*, 2384–2390.

[19] B. A. Johnson, R. A. Blevins, *J. Biomol. NMR* **1994**, *4*, 603–614.

[20] Wüthrich, K. *NMR of Proteins and Nucleic acids*, Wiley-Interscience: New York, **1986**.

[21] D. A. Case, T. A. Darden, T. E. Cheatham, III, C. L. Simmerling, J. Wang, R. E. Duke, R. Luo, M. Crowley, R. C. Walker, W. Zhang, K. M. Merz, B. Wang, S. Hayik, A. Roitberg, G. Seabra, I. Kolossváry, K. F. Wong, F. Paesani, J. Vanicek, X. Wu, S. R. Brozell, T. Steinbrecher, H. Gohlke, L. Yang, C. Tan, J. Mongan, V. Hornak, G. Cui, D. H. Mathews, M. G. Seetin, C. Sagui, V. Babin, and P. A. Kollman, AMBER 10, University of California, San Francisco **2008**.

[22] R. Koradi, M. Billeter, K. Wuthrich, *J. Mol. Graph.* **1996**, *14*, 51–54.

[23] C. E. Dempsey, *J. Am. Chem. Soc.* **1995**, *117*, 7526–7534.

[24] M. C. Burla, R. Caliandro, M. Camalli, B. Carrozzini, G. L. Cascarano, L. De Caro, C. Giacovazzo, G. Polidori, R. Spagna, *J. Appl. Crystallogr.* **2005**, *38*, 381–388.

[25] G. M. Sheldrick, *Acta Crystallogr. Sect. A* **2008**, *64*, 112–122.

[26] Gaussian 09. Revision C.01, Frisch, M. J.; Trucks, G. W.; Schlegel, H. B.; Scuseria, G. E.; Robb, M.; Cheeseman, J. R.; Scalmani, G.; Barone, V.; Mennucci, B.; Petersson, G. A.; Nakatsuji, H.; Caricato, M.; Li, X.; Hratchian, H. P.; Izmaylov, A. F.; Bloino, J.; Zheng, G.; Sonnenberg, J. L.; Hada, M.; Ehara, M.; Toyota, K.; Fukuda, R.; Hasegawa, J.; Ishida, M.; Nakajima, T.; Honda, Y.; Kitao, O.; Nakai, H.; Vreven, T.; Montgomery, Jr. J. A.; Peralta, J. E.; Ogliaro, F.; Bearpark, M.; Heyd, J. J.; Brothers, E.; Kudin, K. N.; Staroverov, V. N.; Keith, T.; Kobayashi, R.; Normand, J.; Raghavachari, K.; Rendell, A.; Burant, J. C.; Iyengar, S. S.; Tomasi, J.; Cossi, M.; Rega, N.; Millam, J. M.; Klene, M.; Knox, J. E.; Cross, J. B.; Bakken, V.; Adamo, C.; Jaramillo, J.; Gomperts, R.; Stratmann, R. E.; Yazyev, O.; Austin, A. J.; Cammi, R.; Pomelli, C.; Ochterski, J. W.; Martin, R. L.; Morokuma, K.; Zakrzewski, V. G.; Voth, G. A.; Salvador, P.; Dannenberg, J. J.; Dapprich, S.; Daniels, A. D.; Farkas, O.; Foresman, J. B.; Ortiz, J. V.; Cioslowski, J. and Fox, D. J.: Gaussian, Inc., Wallingford CT, **2010**.

[27] A. D. Becke, *J. Chem. Phys.* **1993**, *98*, 5648–5652.

[28] AIMAll software, T. A. Keith, TK Gristmill Software, Overland Park KS, USA, 2012 (aim.tkgristmill.com), AIMAll (Version 12.06.03).

[29] E. Espinosa, E. Molins, C. Lecomte, *Chem. Phys. Lett.* **1998**, *285*, 170–173.